m2sv: A Scalable Benchmark for Map-to-Street-View Spatial Reasoning

Yosub Shin [1] **Michael Buriek** [1 2] **Igor Molybog** [1]

Abstract

Vision–language models (VLMs) achieve strong performance on many multimodal benchmarks but remain brittle on spatial reasoning tasks that require aligning abstract overhead representations with egocentric views. We introduce **m2sv**, a scalable benchmark for map-to-street-view spatial reasoning that asks models to infer camera viewing direction by aligning a north-up overhead map with a Street View image captured at the same real-world intersection. We release **m2sv-20k**, a geographically diverse benchmark with controlled ambiguity, along with **m2sv-sft-11k**, a curated set of structured reasoning traces for supervised fine-tuning.

Despite strong performance on existing multimodal benchmarks, the best evaluated VLM achieves only 65.2% accuracy on m2sv, below human annotators who reach 72.0% on average (and 95% for an expert) with strong inter-annotator agreement (κ up to 0.76). While supervised fine-tuning and reinforcement learning yield consistent gains, cross-benchmark evaluations reveal limited transfer. Beyond aggregate accuracy, we systematically analyze *difficulty* in map-to-street-view reasoning using both structural signals and human effort, and conduct an extensive failure analysis of adapted open models. Our findings highlight persistent gaps in geometric alignment, evidence aggregation, and reasoning consistency, motivating future work on grounded spatial reasoning across viewpoints.

1. Introduction

Vision–language models have demonstrated impressive capabilities in object recognition, diagram understanding, and text-heavy multimodal reasoning. However, they continue to struggle with tasks that require consistent spatial grounding across viewpoints. In particular, aligning abstract overhead representations such as maps with egocentric, ground-level imagery remains a fundamental challenge. This capability is essential for applications in navigation, robotics, and embodied assistants, yet is weakly represented in current evaluation benchmarks.

Most existing multimodal reasoning benchmarks emphasize synthetic diagrams, charts, or carefully curated visual puzzles where geometry is simplified or explicitly annotated. Real-world spatial reasoning is substantially harder: it requires coping with viewpoint changes, partial observability, temporal mismatch between data sources, and ambiguity arising from repeated or symmetric structures. As a result, current benchmarks may overestimate spatial competence by avoiding the alignment of disparate viewpoints. We reserve a deeper discussion of related work and background for Appendix A.

In this work, we introduce **m2sv** (map-to-street-view), a benchmark designed to isolate a core spatial reasoning primitive: inferring camera viewing direction by aligning a north-up overhead map with a Street View image captured at the same real-world intersection (Figure 1). Each example requires models to reason about road topology, intersection geometry, and stable landmarks, while ignoring transient or unreliable cues such as vehicles, lighting, or pedestrians. By grounding questions in real-world imagery and geometry, m2sv exposes failure modes that are largely hidden in synthetic or single-view tasks.

Beyond serving as a benchmark, m2sv enables a systematic study of *difficulty* in spatial reasoning. Because intersection geometry and candidate directions are known a priori, we can define scalable structural difficulty signals such as the number of candidate directions and angular symmetry. We complement these with human response-time measurements, allowing us to distinguish between structural ambiguity and human-perceived difficulty. This dual view reveals that even moderate geometric ambiguity induces sharp performance drops in models, while humans remain near ceiling.

Finally, we perform an extensive failure analysis of our best adapted open model, going beyond aggregate accuracy to identify recurring breakdowns such as egocentric–

[1]University of Hawai'i at Mānoa, Honolulu, HI, USA [2]PwC, USA. Correspondence to: Yosub Shin <yosubs@hawaii.edu>.

Accepted to the 1st Workshop on Combining Theory and Benchmarks, CTB@ICML 2026, Seoul, South Korea. Copyright 2026 by the author(s).

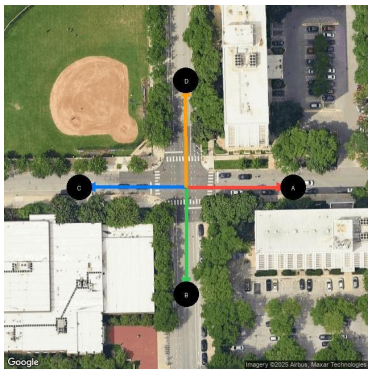

(a) North-up overhead map with labeled candidate directions.

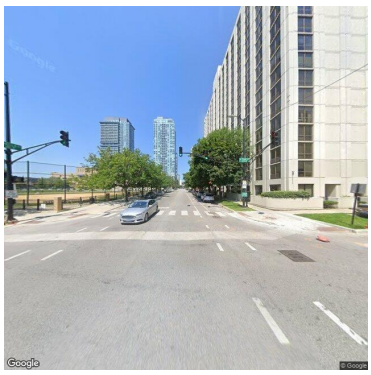

(b) Street View image captured at the same intersection.

Question
Which labeled direction on the map corresponds to the direction in which the street view photo was taken? Options: A, B, C, D.

Generated trace (Gemini-2.5-Pro)
Step 1: Analyze the street-view photo. The photo is taken from the center of an intersection, looking straight ahead. On the immediate right is a very tall, light-colored (white or beige) apartment or office building.
It runs along the street from the corner onwards. On the immediate left is a fenced-off open area, which looks like a park or a sports field.
There are trees lining the sidewalk.
In the distance, further down the road, at least two prominent skyscrapers are visible. The road itself is a multi-lane street.
Step 2: Analyze the overhead map and evaluate each option. The camera is at the central intersection.
Option A (looking East): To the right (south) is a large white building. To the left (north) is another large white building. This does not match the photo, which has a park/field on the left.
Option B (looking South): To the right (west) is a large white building. To the left (east) is another large white building. This does not match the photo.
Option C (looking West): To the right (north) is a large green area with a baseball field. To the left (south) is a large white building. This is the opposite of the street view (building on the right, park on the left).
Option D (looking North): To the right (east) is a long, rectangular, light-colored building located right at the corner. To the left (west) is a large green area containing a baseball field. This arrangement perfectly matches the street-view photo.
Step 3: Conclude the comparison. Direction D is the only view from the intersection that has a large park/baseball field on the left and a tall, long building on the right. Final answer: \boxed{D}.

Ground truth
D

Figure 1. Illustrative m2sv example with paired images and a model-generated reasoning trace. The model correctly infers the viewing direction by aligning stable map geometry with the Street View image.

allocentric confusion, symmetry traps, unreliable cue reliance, and internal reasoning inconsistencies.

Our contributions are:

- A fully automated pipeline for constructing large-scale map-to-street-view spatial reasoning benchmarks, including image data sourcing, candidate response generation, and labeling tools.
- **m2sv-20k**, a geographically diverse benchmark with controlled ambiguity and statistically reliable evaluation, and **m2sv-sft-11k**, a curated set of structured reasoning traces for supervised fine-tuning.
- A systematic characterization of **difficulty in spatial reasoning**, combining structural signals (e.g., number of candidate directions and angular symmetry) with human effort and model behavior (Section 6).
- An extensive evaluation and **failure mode analysis**, identifying recurring breakdowns such as egocentric–allocentric confusion, symmetry traps, unreliable cue reliance, and internal reasoning inconsistencies (Section 7).

Reproducibility and open release. All artifacts are publicly available at our project repository.[1] We release: (i) the **m2sv-20k** blueprints—intersection coordinates, candidate azimuths, ground-truth labels, and Street View panorama identifiers—together with the deterministic rendering pipeline, so the full benchmark can be reconstructed on demand under licensing constraints; (ii) the **m2sv-sft-11k** reasoning traces; (iii) all evaluation and fine-tuning code, including prompts and hyperparameters; and (iv) the interactive human-evaluation interface, hosted live at https://m2sv.yosubshin.com, along with the collected per-item human labels and response times. Together these enable reproduction of the zero-shot, adaptation, and human-baseline results reported in this paper.

2. Benchmark Design

Each m2sv example consists of two images: (1) a north-up overhead map centered at a real-world intersection, anno-

[1] Code, data, and interface: https://github.com/yosubshin/m2sv. Live human-evaluation interface: https://m2sv.yosubshin.com.

tated with labeled directional rays, and (2) a Street View image captured near the same intersection and oriented along one of those rays. The task is to identify which labeled direction corresponds to the Street View camera orientation.

The number of candidate directions per example ranges from 2 to 7, with a median of 3 (mean: 3.24). Accordingly, the random-guess baseline is approximately 31.4%. Accuracy is measured over multiple-choice labels.

3. Dataset and Blueprint Pipeline

3.1. Blueprint specification

We decouple dataset specification from image rendering by releasing blueprint metadata that records intersection coordinates, candidate azimuths, correct labels, and Street View panorama identifiers. Images are rendered on demand using a standardized pipeline, enabling deterministic reconstruction of the dataset.

3.2. Sampling and filtering

Intersections are sampled from a seed list of major metropolitan areas worldwide to encourage broad geographic coverage. The sampling pipeline itself is city-agnostic and can be readily extended to additional regions by modifying the city list.

To control ambiguity and ensure fair evaluation, we apply several filtering criteria. Street View panoramas are restricted to within 5 m of the intersection center, resulting in a tightly controlled offset distribution (median: 2.05 m; 95th percentile: 4.51 m). We further enforce a minimum angular separation of 15° between candidate azimuths to exclude near-collinear road configurations that are difficult even for humans to disambiguate.

3.3. Dataset statistics

m2sv-20k contains 20,000 examples (10k train, 10k validation) spanning 32 cities across multiple continents. Per-city caps prevent over-representation of dense urban areas. The number of candidate directions per example ranges from 2 to 7 (min: 2, max: 7, mean: 3.24, median: 3). Table 3 in the appendix reports additional statistics.

3.4. Reasoning traces

We curate **m2sv-sft-11k**, a subset of 11,000 examples annotated with structured reasoning traces generated by Gemini-2.5-Pro. Traces explicitly compare map geometry and Street View imagery and terminate in a boxed final answer. Fine-tuning on all traces slightly underperformed, so we filter to correct traces only, yielding 4.4k examples total (4.37k train, 485 validation). These traces are used exclusively for supervised fine-tuning experiments.

Table 1. Zero-shot baseline performance on m2sv with 95% confidence intervals. The engaged-human row reports the mean over eight annotators with the between-annotator standard deviation (not a binomial interval).

Model	N	Accuracy (%)
Gemini-3-Pro	1k	65.2 ± 3.0
GPT-5	1k	57.2 ± 3.1
Gemini-2.5-Pro	1k	47.2 ± 3.1
Qwen3-VL-8B-Instruct	1k	35.5 ± 3.0
Qwen3-VL-235B-A22B-Thinking	1k	42.7 ± 3.1
Random baseline	1k	31.4 ± 2.9
Human (engaged, n=8)	200	72.0 ± 9.7
Human (expert)	200	95.0

4. Experimental Setup

We evaluate a range of proprietary and open-source VLMs using a standardized prompt that describes the task and instructs models to ignore transient visual elements. Accuracy and 95% confidence intervals are reported.

We fine-tune from Qwen3-VL-8B-Instruct using LoRA for both SFT and RL. SFT uses the filtered correct-trace subset (4.4k) and LoRA improves accuracy by 1.2% over full-parameter SFT. We train with LR 2e-4, cosine schedule with 0.03 warmup ratio, batch size 4, and early stopping at 2.3 epochs (max 4), using 1xH200 for about 2 hours. RL starts from the SFT checkpoint and uses LoRA with LR 2e-5, generation_batch_size 64, per_device_train_batch_size 16, and gradient_accumulation_steps 16, trained on 2xH200 for about 36 hours; we report results from the step-550 checkpoint.

5. Results

5.1. Zero-shot baselines and the human performance gap

We begin by establishing zero-shot baselines and the human performance ceiling on m2sv. Table 1 reports accuracy for a range of proprietary and open vision–language models evaluated without task-specific adaptation, alongside a random baseline and human performance measured on a 200-example subset.

To establish a robust human reference, we conduct an independent multi-annotator study on the 200-example subset. Twelve annotators—none of whom participated in dataset construction or had prior exposure to the benchmark items[2]—

[2]Eleven are external volunteers; the twelfth is a co-author who

answer items through a web interface that logs the selected option and per-item response time. Ten completed all 200 items and form our analysis set; the remaining two answered only 17 and 76 items and are excluded for comparability (their small overlap also makes pairwise agreement unstable). We additionally retain the original expert annotator (a dataset author) as a ceiling reference.

Human accuracy is high but effort-dependent (Figure 2). Eight mutually consistent annotators average 72.0% (between-annotator SD 9.7%) and the expert reaches 95%, all above the strongest model (Gemini-3-Pro, 65.2%); two annotators answered at or below chance (42% and 22%) and are flagged not by accuracy but by near-zero or negative agreement with every other rater (Cohen's $\kappa \leq 0.15$)—one was fast and one slow, so the exclusion reflects disagreement, not speed. The below-chance annotator's answers were systematically the *opposite* heading (median angular error 150°, negative κ); a debrief traced this to a misunderstood convention—treating the labeled marker as the camera's location rather than the intersection center, which inverts every heading—rather than a spatial-reasoning deficit, plausibly compounded by non-native instructions. Agreement-based exclusion thus removes task misunderstanding that an accuracy threshold alone would conflate with poor spatial ability. Inter-annotator agreement is otherwise moderate to substantial (Figure 3): the expert and the engaged annotators agree well with one another (median pairwise $\kappa = 0.48$, up to 0.76), confirming that the labels are reliable and that attentive humans converge on the same answers. In contrast, Gemini-3-Pro agrees with humans only moderately (median $\kappa = 0.42$, below the human–human median) and Qwen3-VL-235B shows only slight agreement (median $\kappa = 0.15$). The human–model gap is thus visible not only in accuracy but in agreement structure: the best model sits below the human consensus, indicating that zero-shot pretrained VLMs lack robust mechanisms for aligning overhead maps with egocentric street-level views.

5.2. Adaptation baselines on m2sv

We next evaluate whether task-specific adaptation can mitigate this gap. Table 2 reports results for Qwen3-VL-8B under three training regimes: the base model, supervised fine-tuning (SFT) on m2sv reasoning traces, and reinforcement learning (RL) applied on top of SFT.

Supervised fine-tuning yields a consistent improvement over the base model, and reinforcement learning provides an additional gain of approximately four points. These results demonstrate that m2sv-specific supervision teaches useful task structure and improves decision consistency. However, even after SFT and RL, performance remains more than 50 points below the human ceiling, indicating that adaptation alone does not close the gap in spatial alignment capability.

contributed to the reinforcement-learning pipeline but not to the benchmark data or the human-evaluation protocol, and encountered the items for the first time during the study.

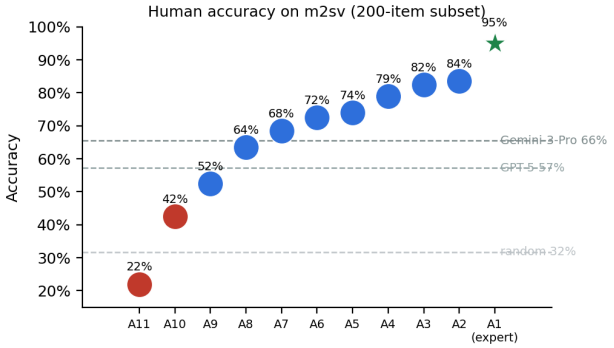

Figure 2. **Per-annotator human accuracy on the 200-example subset** (the ten annotators who completed all 200 items). Annotators span 22%–84%; the two low-agreement outliers ($\kappa < 0.3$ with the expert) are shown in red and the expert as a star. Dashed lines denote model and random baselines.

Table 2. Adaptation results on m2sv-20k (10k validation).

Model	Training	Accuracy (%)
Qwen3-VL-8B	Base	34.3 ± 0.9
Qwen3-VL-8B	SFT	39.8 ± 1.0
Qwen3-VL-8B	SFT+RL	43.9 ± 1.0

5.3. Cross-benchmark transfer

To assess whether improvements on m2sv reflect more general spatial reasoning abilities, we evaluate m2sv-trained models on established multimodal benchmarks. Table 4 in the appendix reports performance on a subset of commonly used benchmarks for Qwen3-VL-8B variants.

Transfer results are mixed and do not show consistent improvements across benchmarks. Some metrics improve under SFT or SFT+RL, while others degrade or remain unchanged. This sensitivity suggests that gains on m2sv do not reliably translate into broader multimodal reasoning improvements, and may instead reflect benchmark-specific adaptations.

5.4. Asymmetric transfer with MindCube

To further probe transferability, we conduct a focused evaluation on the MindCube suite (Yin et al., 2025), which also targets spatial reasoning but differs in input structure and output format. Table 5 in the appendix reports performance under multiple prompting configurations for Qwen3-VL-8B variants.

m2sv-trained models occasionally outperform the base

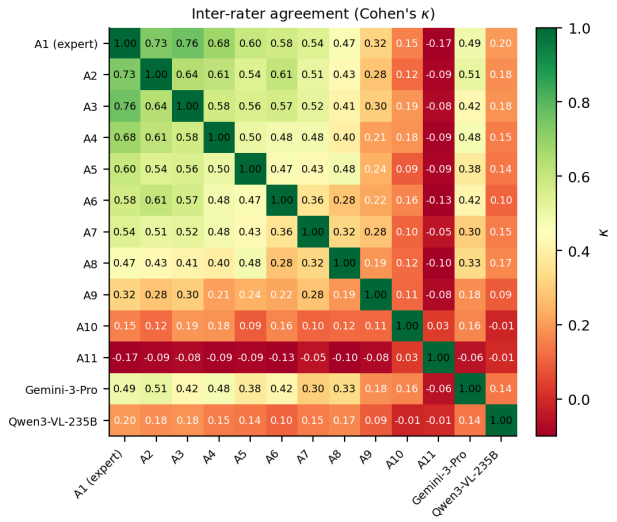

Figure 3. **Inter-rater agreement (Cohen's κ),** chance-corrected per item by candidate count. The expert (A1) and engaged annotators (A2–A9) form a high-agreement block; Gemini-3-Pro sits below the human consensus and Qwen3-VL-235B lower still. The low-agreement annotators (A10, A11) are outliers against all raters.

model on MindCube, but gains are highly sensitive to prompting format and are largest in *direct answer* settings. When explicit reasoning traces are requested, the base model matches or exceeds the adapted variants. Conversely, models trained on MindCube perform near random on m2sv, indicating asymmetric and limited transfer.

Together, these results suggest that current fine-tuning pipelines induce benchmark-specific reasoning policies rather than transferable spatial representations, despite surface-level similarity between tasks.

6. Measuring Difficulty in Map-to-Street-View Reasoning

A central challenge in evaluating spatial reasoning is defining what makes an example *difficult*. In the map-to-street-view task, difficulty does not arise from a single factor but from an interaction between intersection geometry and fine-grained visual confusability across candidate directions. We therefore distinguish between two complementary notions of difficulty: *structural difficulty*, which is automatically measurable and scalable, and *human-perceived difficulty*, which reflects the cognitive effort required to resolve subtle spatial ambiguities. We reflect on the background of vision-language spatial reasoning difficulty analysis in Appendix A.4.

Structural measures are attractive for large-scale dataset analysis and potential curriculum learning, but they are necessarily coarse. Human-perceived difficulty, while expensive to obtain, provides a diagnostic signal that captures visual and semantic factors beyond geometry. We analyze both to characterize where current vision–language models succeed and where they fail.

6.1. Structural difficulty signals

6.1.1. Structural Difficulty via Number of Candidate Directions

We analyze difficulty through a structural lens using the number of candidate directions (#options) provided in each question. This quantity is derived directly from intersection geometry and is available for every example without human annotation, making it a scalable proxy for geometric ambiguity and a natural signal for dataset filtering or curriculum learning.

A direct comparison of raw accuracy across different values of #options is confounded by varying chance levels (e.g., 0.5 for two options vs. 0.25 for four options). To account for this, we report *chance-normalized accuracy gain*, defined as $(a-c)/(1-c)$, where a is model accuracy and $c = 1/K$ is the chance accuracy for K options. This normalization measures how much useful signal a model extracts beyond random guessing.

Figure 4 reports chance-normalized performance as a function of the number of options (2, 3, and 4) for our best open model (Qwen3-VL-8B SFT+RL) evaluated on the full 10k validation set, and for two strong proprietary models evaluated on a 1k subset. This enables a statistically stable, large-scale analysis of structural difficulty.

Across all models, normalized performance does *not* degrade monotonically with the number of options. Instead, three-option intersections yield the highest normalized gains, outperforming both two- and four-option cases. This pattern is consistent across open and proprietary systems and reflects the role of geometric asymmetry: three-way intersections are often T-junctions with distinctive spatial layouts, whereas two- and four-way intersections are more likely to be symmetric and thus ambiguous.

These results demonstrate that the number of candidate directions alone is an incomplete measure of structural difficulty. Intersection cardinality interacts with geometric symmetry, and higher difficulty arises not simply from having more choices, but from the absence of asymmetry that can break directional ambiguity. This motivates the finer-grained structural and perceptual difficulty analyses that follow.

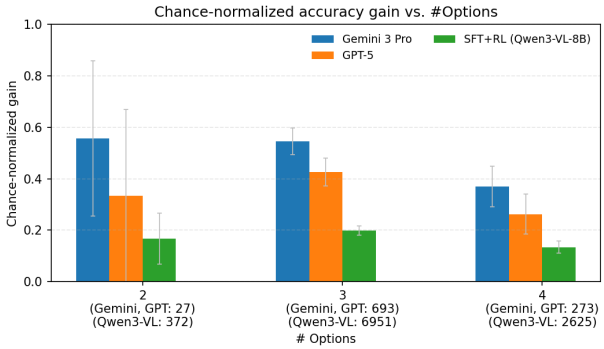

Figure 4. **Chance-normalized accuracy vs. structural difficulty.** Accuracy normalized by chance level as a function of the number of candidate directions (#options). Qwen3-VL-8B (SFT+RL) is evaluated on the full 10k validation set, while Gemini 3 Pro and GPT-5 are evaluated on a 1k subset. Three-option intersections yield the highest normalized gains across models, reflecting the benefit of geometric asymmetry. Error bars denote 95% binomial confidence intervals.

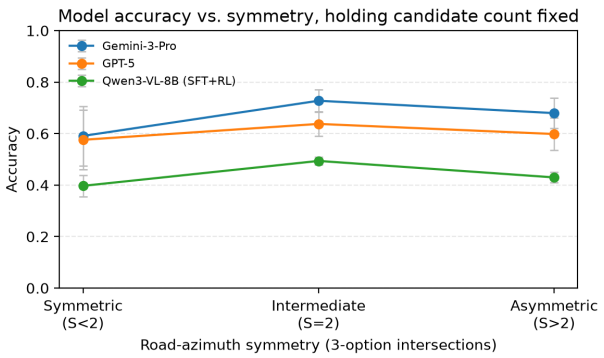

Figure 5. **Model accuracy vs. road-azimuth symmetry (three-option intersections).** Accuracy by symmetry level S (Eq. 2) with candidate count held fixed, removing the confound between symmetry and the number of options. All three models are hardest on symmetric ($S < 2$) intersections and peak at intermediate symmetry ($S = 2$). Error bars denote 95% binomial confidence intervals.

6.1.2. Structural Ambiguity via Road-Azimuth Symmetry

The number of options captures how many candidate directions are present, but not how *interchangeable* those directions are. To refine the notion of structural difficulty, we introduce a road-azimuth symmetry measure based on the angular spacing between candidate directions. Intersections with evenly spaced azimuths (e.g., four-way junctions) are geometrically symmetric, while those with highly uneven spacing exhibit a dominant road direction and are structurally asymmetric.

Concretely, let $\theta_1 \leq \cdots \leq \theta_K$ be the K candidate azimuths (in degrees) sorted on the circle, and define the K consecutive angular gaps

$$g_i = \theta_{i+1} - \theta_i \;\; (1 \leq i < K), \qquad g_K = 360^\circ + \theta_1 - \theta_K, \tag{1}$$

where g_K is the wrap-around gap. We define the *road-azimuth symmetry* of an intersection as the ratio of its largest to smallest gap,

$$S = \frac{\max_i g_i}{\min_i g_i} \geq 1. \tag{2}$$

A regular intersection with evenly spaced rays has $S = 1$ (maximally symmetric), whereas a dominant-road layout containing one large gap has $S \gg 1$ (asymmetric). Two properties of S require care. First, because candidate azimuths are coarsely quantized, S takes few distinct values—a single value $S = 2$ accounts for nearly half of all three-option intersections—so fine-grained quantile binning arbitrarily splits ties. Second, symmetry is correlated with candidate count: the most symmetric intersections ($S \approx 1$) are overwhelmingly four-way junctions. To avoid both pitfalls, we hold candidate count fixed—analyzing the three-option stratum, the largest group—and bin into three well-separated, untied levels: *Symmetric* ($S < 2$), *Intermediate* ($S = 2$), and *Asymmetric* ($S > 2$).

Figure 5 reports model accuracy across these bins. Even with candidate count held fixed, accuracy is non-monotonic in symmetry: all three models are hardest on the most *symmetric* intersections (e.g., Gemini-3-Pro 59% vs. 73% at intermediate symmetry), with a smaller decline toward the most asymmetric layouts. The dip at high symmetry is consistent across open and proprietary systems, confirming that near-even (Y-shaped) intersections are genuinely the most confusable rather than an artifact of candidate count.

This pattern indicates that azimuth symmetry is a real but non-monotonic driver of difficulty. Near-even intersections offer no dominant road to anchor the candidate directions and are the hardest; a single straight through-road (intermediate symmetry) is the most recognizable; and strongly dominant-road layouts are slightly harder again. Symmetry thus bounds difficulty without fully determining it.

6.2. Human effort as a difficulty proxy

Structural measures do not capture visual confusability between candidate directions, which often determines whether fine-grained spatial alignment is required. To probe these effects directly, we analyze difficulty as perceived by human annotators, using response time as a proxy for cognitive effort.

Using the multi-annotator study of Section 5.1, we record per-item response time for every annotator on the 200-example subset. Unlike models, humans show no symmetry-dependent slowdown: per-problem median response time is

essentially flat across symmetry (∼15 s in every three-option symmetry bin), so humans resolve symmetric and asymmetric intersections with comparable effort even though models collapse on the symmetric ones (Figure 5).

Figure 6 instead uses response time as a global difficulty signal: examples are partitioned into tertiles by the *median* response time across the engaged annotators who completed all 200 items (the median is robust to occasional idle responses, which the visibility detector cannot catch). This difficulty axis is a purely human-effort signal, computed without reference to any model, so the model accuracy curves—and hence the human–model gap—cannot be artifacts of how difficulty is defined. Taking the median across many annotators, rather than relying on a single rater's latency as in our pilot, also removes the within-subject coupling between one rater's per-trial speed and correctness that would otherwise be conflated with item difficulty. The human accuracy curve is shown for reference: that effort and accuracy co-vary within the same annotators is expected and is not the claim we draw from this figure. Humans degrade gently with difficulty (83% to 63%) and remain well above both models on every tier; the models, by contrast, lose the most ground precisely on the hardest examples. Gemini-3-Pro degrades more steeply than humans at *both* steps (82% → 65% → 50%), so the human–model gap widens monotonically—Gemini nearly matches humans on the easiest tier but trails by 13 points on the hardest. Qwen3-VL-235B (Thinking) instead holds roughly flat through the easy and medium tiers (50%, 48%) and then collapses to chance on the hardest tier (31% vs. ∼30%); its degradation is concentrated entirely in the hard regime, where humans still reach 63%. The common pattern is thus a hardest-tier collapse: both models fall to (Qwen) or toward (Gemini) chance exactly where fine-grained spatial alignment is most required, while humans hold up. Candidate-count composition is similar across bins, so chance is ∼30–32% in all three tiers.

Taken together, these results suggest that model failures are driven not by geometry alone, but by an inability to exploit subtle, stable cues when visual ambiguity remains high. While structural asymmetry allows humans to shortcut the alignment process, current vision–language models do not reliably adapt their inference strategy to difficulty, motivating future work on difficulty-aware training and adaptive inference.

6.3. Model behavior vs. difficulty

We analyze how models modulate the length of their reasoning traces as a function of problem difficulty. As the difficulty axis we reuse the same multi-annotator median-response-time tertiles as Figure 6. Trace length is measured as the approximate number of generated tokens in the model's reasoning output.

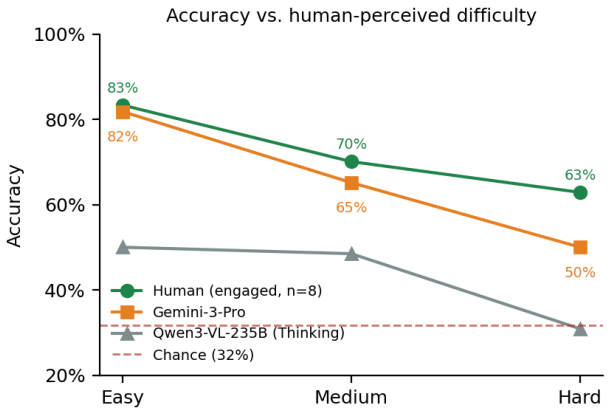

Figure 6. **Accuracy vs. human-perceived difficulty (multi-annotator).** Examples are partitioned into Easy/Medium/Hard tertiles by *median* response time across the engaged annotators who completed all 200 items. The difficulty axis is a human-effort signal independent of any model, so the model curves and the widening gap are not artifacts of the binning; the human curve is shown for reference. Humans degrade gently and stay above both models on every tier; both models lose the most ground on the hardest tier—Gemini-3-Pro falls toward, and Qwen3-VL-235B to, chance—where the human–model gap is largest.

Figure 7 reports average trace length across difficulty buckets (easy, medium, hard) for proprietary models and multiple variants of Qwen3-VL. We exclude GPT-5 from this analysis, as we observed that it does not reliably produce explicit reasoning traces and often responds with a direct answer only, making trace-length measurements inconsistent.

Gemini 3 Pro expands its reasoning on harder examples, increasing trace length monotonically across difficulty; Qwen3-VL-235B (Thinking) trends upward overall but less cleanly. The base Qwen3-VL-8B Instruct model produces long traces but without a consistent difficulty trend.

In contrast, both the supervised fine-tuned Qwen3-VL-8B (SFT) and the Qwen3-VL-8B (SFT+RL) models produce *markedly shorter and nearly constant-length* traces across difficulty levels. Adaptation thus compresses reasoning toward a short, fixed budget rather than preserving the difficulty-adaptive expansion exhibited by the strongest model, even though overall accuracy improves.

Taken together, trace length modulation and task accuracy appear to be separable capabilities. Stronger proprietary models retain both difficulty awareness and effective multi-cue integration, while adapted open models achieve higher accuracy at the cost of reduced adaptive reasoning depth. This behavior aligns with the failure modes identified in Section 7, where adapted models often commit prematurely under symmetry or rely on a single dominant feature instead of escalating to finer-grained spatial evidence.

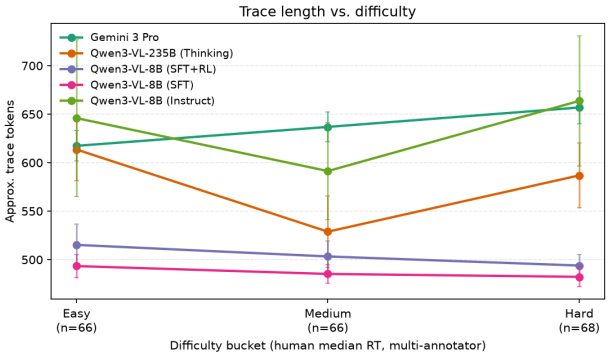

Figure 7. **Reasoning trace length vs. difficulty.** Average trace length (in tokens) as a function of difficulty (multi-annotator median-response-time tertiles, the same bins as Figure 6). Gemini 3 Pro and Qwen3-VL-235B (Thinking) increase trace length on harder examples, while Qwen3-VL-8B models adapted via SFT and SFT+RL produce near-constant-length traces despite higher accuracy. Error bars denote standard error of the mean.

7. Failure Mode Analysis

To better understand why current vision–language models fail on m2sv despite strong zero-shot performance on other multimodal benchmarks, we conduct a qualitative failure analysis on a subset of challenging examples. Rather than attempting an exhaustive taxonomy, we focus on a small number of recurring failure patterns that consistently appear across models and difficulty regimes.

Importantly, these failures do not reflect fundamentally unsolvable cases: human annotators are able to solve nearly all examples, often by investing additional effort and exploiting subtle but stable spatial cues. Model errors instead arise from brittle alignment strategies and inappropriate reliance on unreliable visual evidence.

Below, we summarize common failure modes observed in both open and proprietary models, illustrated with representative examples.

Egocentric–allocentric confusion (left–right inversion). Models frequently misinterpret the relationship between egocentric directions in the street-view image and allocentric directions on the overhead map. This often manifests as left–right inversions, where a correct identification of landmarks is followed by an incorrect mapping to map orientation, particularly at four-way intersections (Fig. 8a).

Over-reliance on unreliable cues. In many failures, models base eliminations on visually salient but unstable cues such as roof color, shadows, lighting conditions, or image blur. These cues are often weakly or not at all represented in overhead imagery and can vary substantially with capture time, leading to confident but incorrect conclusions (Fig. 8b).

Landmark misbinding. Models sometimes correctly identify salient landmarks in the overhead view but misassociate them with the wrong candidate direction or parcel. For example, a swimming pool visible several houses away may be incorrectly attributed to the immediate intersection, leading to erroneous eliminations. This suggests limited precision in spatial binding between landmarks and their local context (Fig. 8c).

False landmark projection. In other cases, models introduce landmarks that are not present within the local intersection context, such as distant structures or perspective-induced artifacts. These projected landmarks are then treated as decisive evidence, despite lacking support in the overhead map, indicating weak control over spatial scope and relevance (Fig. 9d).

Failure to maintain a consistent spatial representation. In some failures, models do not maintain globally consistent spatial properties across options, treating shared structures as independent entities. This can manifest as assigning different road widths, lane counts, or landmark layouts to opposite headings of the same road, or contradicting earlier correct spatial descriptions during later reasoning. These errors suggest that models evaluate options in isolation rather than constructing and enforcing a coherent global spatial model (Fig. 9a).

Internal contradiction and state inconsistency. In some failures, models correctly identify spatial relationships or landmark configurations, but subsequently contradict themselves while reasoning or verbalizing the solution. These errors are characterized by internally inconsistent statements (e.g., asserting a correct left–right relation and then rejecting it), even though the underlying spatial alignment is correct. Unlike egocentric–allocentric confusion, these failures arise from an inability to maintain and consistently apply inferred spatial commitments across reasoning steps (Fig. 9b).

Symmetry traps and insufficient cue escalation. At symmetric or near-symmetric intersections, models often identify multiple plausible candidate directions but fail to escalate to finer-grained geometric cues—such as lane counts, road markings, curb geometry, or persistent vegetation—that would resolve the ambiguity. Instead, models rely on weak or unstable evidence and prematurely eliminate the correct option (Fig. 9c).

7.1. Implications.

Taken together, our analyses suggest that model failures on m2sv are not driven primarily by geometric complexity or lack of visual information, but by an inability to adapt inference strategies to the level of ambiguity present in an

example. Structural asymmetry allows humans to shortcut reasoning on easy cases, while symmetric or visually confusable cases trigger deeper, more careful comparison. Current vision–language models, by contrast, exhibit relatively uniform reasoning behavior across difficulty regimes, leading to brittle decisions when subtle spatial cues are required.

This gap highlights an important limitation of current training and inference pipelines: models do not reliably escalate their reasoning depth or evidence aggregation in response to increased difficulty. Addressing this limitation may require difficulty-aware training curricula, adaptive inference mechanisms, or explicit modeling of uncertainty in spatial alignment tasks.

8. Limitations and Future Work

m2sv relies on the availability and coverage of commercial mapping services and consequently inherits biases from their data collection practices, including uneven geographic coverage and representation. The benchmark is restricted to public road intersections and does not include private, restricted, or sensitive locations.

Our human evaluation comprises ten annotators together with one expert on the 200-example analysis subset, with inter-annotator agreement reported in Section 5.1. While this is sufficient to characterize between-annotator variance and to de-confound the response-time difficulty analysis, the annotator pool remains modest and was recruited opportunistically rather than through a controlled, pre-registered protocol; a larger and more demographically balanced study would further strengthen the human reference. We release both the interactive labeling interface (hosted live at https://m2sv.yosubshin.com) and the collected labels, including per-item response-time metadata, to facilitate such larger-scale human studies and alternative analyses of spatial reasoning difficulty.

Our transfer experiments are limited in scope and focus on generalization to a single adjacent benchmark (MindCube). Other relevant benchmarks were not incorporated into our initial experimental setup, either because they were not publicly available at the time (e.g., CityCube) or were released shortly before our experiments and follow different evaluation protocols (e.g., Ego3D-Bench, UrBench). Extending transfer evaluations to additional spatial reasoning and cross-view benchmarks remains an important direction for future work.

9. Conclusion

m2sv provides a scalable benchmark for evaluating map-to-street-view spatial reasoning under real-world conditions. Despite strong performance on existing multimodal benchmarks, vision–language models remain far below human accuracy on this task, with failures increasing sharply under geometric ambiguity and symmetry. Our analyses show that these errors are not solely due to missing knowledge, but to difficulties in maintaining consistent allocentric–egocentric representations and reasoning under uncertainty. By isolating this core alignment primitive and characterizing both difficulty and failure modes, m2sv serves as a diagnostic complement to existing spatial benchmarks and highlights open challenges for grounded spatial reasoning.

Acknowledgments

This work was supported by the National Science Foundation NRT-AI 2244574.

This work used cloud GPU resources at NCSA Delta cluster through allocation number CIS240027 from the Advanced Cyberinfrastructure Coordination Ecosystem: Services & Support (ACCESS) program, which is supported by National Science Foundation grants # 2138259, # 2138286, # 2138307, # 2137603, and # 2138296.

The technical support and advanced computing resources from University of Hawaii Information Technology Services – Research Cyberinfrastructure, funded in part by the National Science Foundation CC* awards # 2201428 and # 2232862 are gratefully acknowledged.

This material is based upon work supported by the National Science Foundation CISE Graduate Fellowships under Grant # 2313998. Any opinions, findings, and conclusions or recommendations expressed in this material are those of the author(s) and do not necessarily reflect the views of the National Science Foundation.

References

Gholami, M., Rezaei, A., Weimin, Z., Mao, S., Zhou, S., Zhang, Y., and Akbari, M. Spatial reasoning with vision-language models in ego-centric multi-view scenes, 2025. URL https://arxiv.org/abs/2509.06266.

Hu, B., Li, H., Bu, S., Chen, L., and Han, P. Oriloc: Unlimited-fov and orientation-free cross-view geolocalization. *IEEE Journal of Selected Topics in Applied Earth Observations and Remote Sensing*, 18:15508–15522, 2025. doi: 10.1109/JSTARS.2025.3579740.

Huang, G., Zhou, Y., Zhao, L., and Gan, W. Cv-cities: Advancing cross-view geo-localization in global cities. *IEEE Journal of Selected Topics in Applied Earth Observations and Remote Sensing*, 2024.

Li, Z., Grossman, M., Qasemi, E., Kulkarni, M., Chen, M., and Chiang, Y.-Y. Mapqa: Open-domain geospatial question answering on map data. *arXiv preprint arXiv:2503.07871*, 2025.

Liu, L. and Li, H. Lending orientation to neural networks for cross-view geo-localization. In *The IEEE Conference on Computer Vision and Pattern Recognition (CVPR)*, June 2019.

Lu, P., Bansal, H., Xia, T., Liu, J., Li, C., Hajishirzi, H., Cheng, H., Chang, K.-W., Galley, M., and Gao, J. Mathvista: Evaluating mathematical reasoning of foundation models in visual contexts. In *International Conference on Learning Representations (ICLR)*, 2024. Oral presentation.

Shepard, R. N. and Metzler, J. Mental rotation of three-dimensional objects. *Science*, 171(3972):701–703, 1971.

Shi, Y., Yu, X., Campbell, D., and Li, H. Where am i looking at? joint location and orientation estimation by cross-view matching. In *IEEE/CVF Conference on Computer Vision and Pattern Recognition (CVPR)*, pp. 4064–4072, 2020.

Shore, T., Mendez, O., and Hadfield, S. Spagbol: Spatial-graph-based orientated localisation. In *IEEE/CVF Winter Conference on Applications of Computer Vision (WACV)*, 2025.

Workman, S., Souvenir, R., and Jacobs, N. Wide-area image geolocalization with aerial reference imagery. In *2015 IEEE International Conference on Computer Vision (ICCV)*, pp. 3961–3969, 2015. doi: 10.1109/ICCV.2015.451.

Xu, H., Hu, Y., Zhu, Z., Gao, C., Wang, Z., Rao, J., Lu, W., Li, W., Yin, Q., and Li, Y. Citycube: Benchmarking cross-view spatial reasoning on vision-language models in urban environments, 2026. URL https://arxiv.org/abs/2601.14339.

Yin, B., Wang, Q., Zhang, P., Zhang, J., Wang, K., Wang, Z., Zhang, J., Chandrasegaran, K., Liu, H., Krishna, R., Xie, S., Li, M., Wu, J., and Fei-Fei, L. Spatial mental modeling from limited views. *arXiv preprint arXiv:2506.21458*, 2025.

Zheng, Z., Wei, Y., and Yang, Y. University-1652: A multi-view multi-source benchmark for drone-based geo-localization. In *ACM International Conference on Multimedia*, 2020.

Zhou, B., Yang, H., Chen, D., Ye, J., Bai, T., Yu, J., Zhang, S., Lin, D., He, C., and Li, W. Urbench: A comprehensive benchmark for evaluating large multimodal models in multi-view urban scenarios, 2025. URL https://arxiv.org/abs/2408.17267.

Zhu, S., Yang, T., and Chen, C. Revisiting street-to-aerial view image geo-localization and orientation estimation. In *IEEE/CVF Winter Conference on Applications of Computer Vision (WACV)*, pp. 756–765, 2021a.

Zhu, S., Yang, T., and Chen, C. Vigor: Cross-view image geo-localization beyond one-to-one retrieval. In *IEEE/CVF Conference on Computer Vision and Pattern Recognition (CVPR)*, 2021b.

A. Background and Related Benchmarks

This appendix situates **m2sv** among recent benchmarks for spatial reasoning and cross-view understanding. We focus on the benchmarks most adjacent to **m2sv** and clarify how our task differs from them.

A.1. What Spatial Capability Does m2sv Measure?

m2sv isolates a single spatial reasoning primitive: *inferring camera heading by aligning an egocentric street-level view with a north-up overhead map at a known location*. Each example fixes the geographic position and varies only the candidate viewing direction, converting orientation from a nuisance variable into the primary reasoning target. This formulation removes global localization and retrieval from the task, forcing explicit reasoning about road topology, landmark placement, and allocentric–egocentric transformations under real-world ambiguity.

A.2. Closest Related Benchmarks

CityCube. CityCube (Xu et al., 2026) benchmarks cross-view spatial reasoning in urban environments and reports recurring failures such as directional confusion and viewpoint inconsistency. Compared to CityCube's broader suite of tasks, **m2sv** intentionally constrains the problem to a *single-step heading decision at a fixed location*, enabling controlled measurement of how structural ambiguity (e.g., symmetry) affects orientation inference.

UrBench. UrBench (Zhou et al., 2025) is a multi-view urban benchmark covering diverse task types (including tasks related to localization and orientation in urban scenes). While UrBench contains cross-view components that are conceptually adjacent to **m2sv**, its scope spans multiple urban reasoning dimensions. In contrast, **m2sv** focuses narrowly on *heading inference* by aligning an overhead map with a Street View observation at a known intersection, thereby isolating allocentric–egocentric alignment as the primary bottleneck.

MindCube. MindCube (Yin et al., 2025) evaluates whether VLMs can maintain coherent spatial mental models from limited observations, including perspective-taking and consistency under viewpoint changes. It motivates "map-then-reason" style approaches that explicitly produce intermediate spatial representations before answering. Although m2sv shares the theme of viewpoint-consistent spatial reasoning, **m2sv** differs in its *real-world cross-view* setting (overhead map $\leftrightarrow$ street-level imagery) and its emphasis on resolving ambiguous cross-view alignment by escalating from coarse, unreliable cues to finer-grained spatial evidence at a concrete intersection.

Ego3D-Bench. Ego3D-Bench (Gholami et al., 2025) evaluates outdoor spatial reasoning using ego-centric, multi-view observations and shows a substantial human–model gap. The associated Ego3D-VLM framework improves performance by introducing an explicit cognitive-map style intermediate representation derived from estimated 3D coordinates. These results support the broader hypothesis that structured intermediate spatial state can benefit VLM reasoning; however, whether similar representations help **m2sv** depends on how well they align to the map–street-view transformation and the uncertainty/ambiguity present in real Street View observations.

A.3. Relation to Cross-View Geo-Localization (CVGL)

Cross-view geo-localization (CVGL) studies the correspondence between ground-level imagery (e.g., street-view panoramas or limited-FoV views) and overhead imagery (e.g., satellite/aerial), with the dominant formulation cast as *retrieval*: a ground query is matched against a geo-tagged overhead database and evaluated using retrieval metrics such as Recall@K (e.g., on CVUSA/CVACT-style benchmarks and follow-ups) (Workman et al., 2015; Liu & Li, 2019; Zhu et al., 2021b; Huang et al., 2024). While some benchmarks extend viewpoints (Zheng et al., 2020), the core objective in these settings remains location retrieval rather than isolating directional reasoning.

Because cross-view appearance and geometry differ substantially, many CVGL methods incorporate mechanisms to account for unknown *orientation/alignment* between ground and overhead views. Representative approaches include explicitly encoding orientation cues (Liu & Li, 2019), using polar transforms and correlation-style matching to estimate azimuth alignment during localization (Shi et al., 2020), or estimating cross-view alignment/orientation as part of the matching pipeline (Zhu et al., 2021a). Recent work also explores graph-structured urban priors and bearing-aware filtering on top of retrieval (Shore et al., 2025), and orientation-free formulations for cross-view matching have been proposed (Hu et al., 2025). However, even when orientation is modeled or estimated, it is typically *in service of improving retrieval*, i.e., heading is not the primary target variable.

m2sv complements CVGL by *fixing the location* and asking the model to infer *orientation directly*. This inversion removes global retrieval shortcuts (e.g., relying on distinctive place identity in a large gallery) and makes directional reasoning the dominant challenge.

A.4. Structural Difficulty and Symmetry

Unlike many recent vision–language benchmarks, which define difficulty primarily through semantic complexity or multi-step reasoning, spatial reasoning difficulty has a long

Table 3. Summary statistics of the m2sv-20k dataset.

Statistic	Value
Number of examples	20,000
Number of cities	32
Candidate directions (median)	3
Street View distance (median)	2.05 m
Street View distance (95%)	4.51 m

Table 4. Cross-benchmark evaluation for Qwen3-VL-8B variants.

Model	MMMU	MME-Cog/Per	MMStar	Omni3D
Base	0.556	643 / 1721	0.604	0.388
SFT	0.574	501 / 1525	0.574	0.372
SFT+RL	0.563	550 / 1670	0.644	–

history of being operationalized through geometric transformation. In cognitive psychology, difficulty is closely linked to mental effort and response time (RT): classic results show that RT increases linearly with the angular displacement required to align two objects, suggesting a process akin to physical mental rotation (Shepard & Metzler, 1971). By contrast, contemporary VLM benchmarks often categorize difficulty by reasoning depth or semantic richness (e.g., number of symbols, hops, or compositional steps), as in MathVista (Lu et al., 2024) or MapQA (Li et al., 2025), potentially underrepresenting the role of intrinsic geometric ambiguity.

m2sv introduces *structural difficulty* rooted in intersection geometry and symmetry. Symmetric or near-symmetric intersections induce multiple plausible orientations at a coarse level, creating "symmetry traps" that cannot be resolved by semantic pattern matching alone. Breaking these traps requires escalation to finer-grained spatial cues (e.g., lane markings, curb geometry, subtle landmark placement), a process that mirrors increased human RT in geometric alignment tasks. This framing connects classic findings on mental rotation to modern observations of allocentric–egocentric failures in VLMs, and isolates a form of difficulty that is intrinsic to the scene structure itself.

Table 5. MindCube evaluation suite with varying input/output formats.

Input	Output Format	Base	SFT	SFT+RL
Raw + q	Aug + rsn → ans	34.5	34.0	33.2
Aug. + QA	Direct answer	24.6	37.6	41.0
Aug. + QA	Rsn → answer	46.9	40.3	46.1
Raw + q	Rsn → answer	38.5	36.8	36.6
Raw + q	Map + rsn → ans	34.7	33.5	35.2
Raw + q	Direct answer	27.0	34.9	34.7

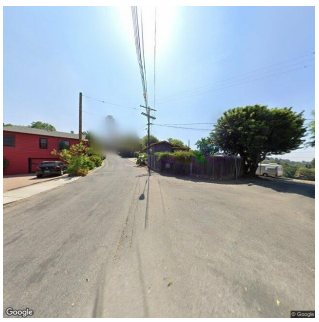

Ground truth: A, **Prediction:** C

Model trace (excerpt):
Looking from the center towards A, the road curves to the right. This contradicts the left curve seen in the photo.

Failure: Egocentric–allocentric left/right inversion: Overhead map shows a left curve, but model reasons as if it were a right curve.

(a) Egocentric–allocentric confusion (left–right inversion)

Ground truth: B, **Prediction:** D

Model trace (excerpt):
Looking south from the center, the buildings on both corners appear to have gray roofs. There is no prominent reddish-orange house on the left corner as seen in the photo. Therefore, B is incorrect.

Failure: The Street View angle of the roof is shallow, and the roof color is lighting-dependent. Humans would discount this cue.

(b) Over-reliance on unreliable visual cues

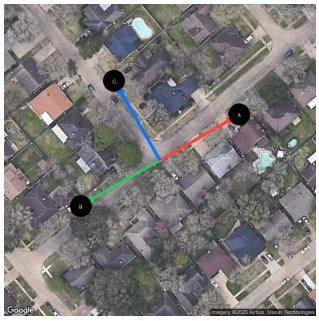

Ground truth: A, **Prediction:** B

Model trace (excerpt):
Facing direction A (east), we look down a relatively straight road. To the immediate left (north) of this view is a corner lot. The house on this corner has a large swimming pool in its backyard. This does not match the houses seen in the street view, which do not have prominent pools immediately adjacent to the road like this one does.

Failure: The corner house does not have a pool, but a pool exists two houses down. The model misattributes a nearby landmark to the wrong spatial anchor.

(c) Landmark misbinding

Figure 8. **Representative qualitative failure modes on m2sv.** Each row shows the same map–street-view pair with a different erroneous reasoning pattern exhibited by the model. From left to right: overhead map with candidate directions, corresponding street-view image, and an excerpt from the model's reasoning trace highlighting the incorrect assumption. All examples are correctly solved by human annotators.

Ground truth: A, **Prediction:** C

Model trace (excerpt):
Direction A: This arrow points east-southeast down a relatively narrow residential street. It has no crosswalks visible across its width. Direction C: This arrow points west-northwest down a much wider road than A and B. This main road clearly has multiple lanes separated by what appear to be painted lines, indicating it's a major thoroughfare. Crosswalks are visible crossing this road.

Failure: A and C are two sides of the same street so the road width is the same, but the answer emphasizes the road width as the key factor

(a) Failure to maintain a consistent spatial representation

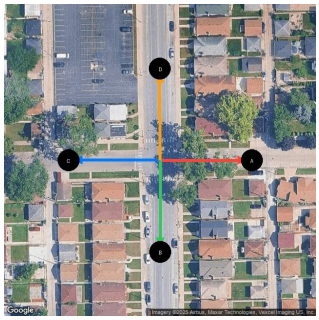

Ground truth: D, **Prediction:** C

Model trace (excerpt):
Option D: This view looks up the main, wide road. On the northeast corner (on the right), there is a residential house. On the northwest corner (on the left), there is the commercial building. This arrangement is the opposite of what is seen in the street view photo, where the commercial building is on the left and the house is on the right.

Failure: The model correctly identifies left–right relationships but subsequently contradicts its own assignments, losing track of spatial state during verbalization.

(b) Internal contradiction and state inconsistency

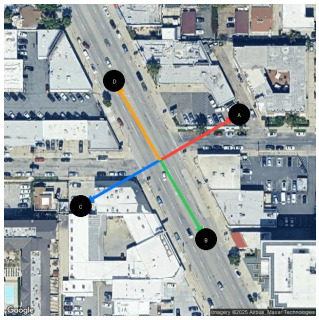
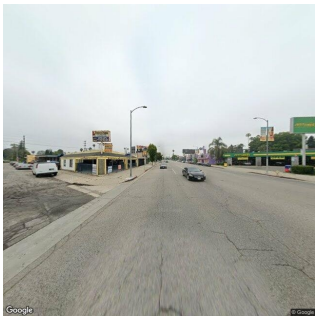

Ground truth: D, **Prediction:** B

Model trace (excerpt):
For view B: Left = Building A, Right = Long Rectangular Building. For view D: Left = Large Building with Parking Lot, Right = Building A. Comparing the photo to view B: We see a specific yellowish building on the left and a gas station on the right.

Failure: The model correctly narrows the decision to two symmetric candidates (B and D), but fails to use subtle geometric cues—such as building orientation relative to the road—to break symmetry, instead introducing unsupported semantic evidence (e.g., a gas station).

(c) Symmetry traps and insufficient cue escalation.

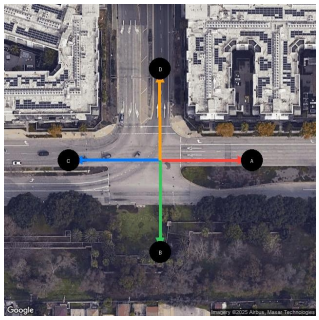

Ground truth: D, **Prediction:** A

Model trace (excerpt):
Direction A provides the most complete match. It correctly places large buildings on both sides of the road and crucially includes the distant underpass/bridge structure that is clearly visible in the street view photo.

Failure: The model invents or misattributes a nonexistent large-scale structure (underpass/bridge) and then reasons as if it were present in the map.

(d) False landmark projection

Figure 9. **More qualitative failure modes on m2sv.** Each row shows the same map–street-view pair with a different erroneous reasoning pattern exhibited by the model. From left to right: overhead map with candidate directions, corresponding street-view image, and an excerpt from the model's reasoning trace highlighting the incorrect assumption. All examples are correctly solved by human annotators.